



**HAL**  
open science

## Optimisation of composite structures – Enforcing the feasibility of lamination parameter constraints with computationally-efficient maps

Terence Macquart, Vincent Maes, Marco Tito Bordogna, Alberto Pirrera, Paul Weaver

### ► To cite this version:

Terence Macquart, Vincent Maes, Marco Tito Bordogna, Alberto Pirrera, Paul Weaver. Optimisation of composite structures – Enforcing the feasibility of lamination parameter constraints with computationally-efficient maps. *Composite Structures*, 2018, 192, pp.605-615. 10.1016/j.compstruct.2018.03.049 . hal-02099784

**HAL Id: hal-02099784**

**<https://hal.science/hal-02099784>**

Submitted on 15 Apr 2019

**HAL** is a multi-disciplinary open access archive for the deposit and dissemination of scientific research documents, whether they are published or not. The documents may come from teaching and research institutions in France or abroad, or from public or private research centers.

L'archive ouverte pluridisciplinaire **HAL**, est destinée au dépôt et à la diffusion de documents scientifiques de niveau recherche, publiés ou non, émanant des établissements d'enseignement et de recherche français ou étrangers, des laboratoires publics ou privés.

## Accepted Manuscript

Optimisation of Composite Structures - Enforcing the Feasibility of Lamination  
Parameter constraints with Computationally-efficient Maps

T. Macquart, V. Maes, Marco T. Bordogna, A. Pirrera, P.M. Weaver

PII: S0263-8223(17)33277-4

DOI: <https://doi.org/10.1016/j.compstruct.2018.03.049>

Reference: COST 9496

To appear in: *Composite Structures*



Please cite this article as: Macquart, T., Maes, V., Bordogna, M.T., Pirrera, A., Weaver, P.M., Optimisation of Composite Structures - Enforcing the Feasibility of Lamination Parameter constraints with Computationally-efficient Maps, *Composite Structures* (2018), doi: <https://doi.org/10.1016/j.compstruct.2018.03.049>

This is a PDF file of an unedited manuscript that has been accepted for publication. As a service to our customers we are providing this early version of the manuscript. The manuscript will undergo copyediting, typesetting, and review of the resulting proof before it is published in its final form. Please note that during the production process errors may be discovered which could affect the content, and all legal disclaimers that apply to the journal pertain.

# Optimisation of Composite Structures - Enforcing the Feasibility of Lamination Parameter constraints with Computationally-efficient Maps

T. Macquart<sup>1</sup>, V. Maes<sup>2</sup>, Marco T. Bordogna<sup>3</sup>, A. Pirrera<sup>4</sup>, P. M. Weaver<sup>5</sup>

---

## Abstract

Composite materials are increasingly used in high performance structural applications because of their high strength and stiffness to weight ratios together with their significant tailoring capabilities. The stiffness of a monolithic laminate can be expressed as a linear combination of material invariants, one thickness variable, and twelve lamination parameters, which is an efficient alternative to using fibre angles as design variables. However, feasibility constraints originating from the interdependency between lamination parameters must be satisfied to obtain laminates with realistic stiffness properties. Currently, enforcing these feasibility constraints is a computationally intensive task. In this paper we propose to use normalised design variables that inherently map (i.e. correspond) to feasible lamination parameters, effectively removing the need to evaluate feasibility constraints altogether. To this end, linear and B-spline maps of the feasible lamination parameter subspace are proposed and evaluated. Results of 2D and 4D benchmark analyses and optimisation studies suggest that the proposed methodology does successfully provide an efficient means of achieving feasible results at lower computational costs.

*Keywords:* Composite Materials, Laminate, Structural Optimisation, Lamination Parameters, Maps

---

## 1. Introduction

Over the last decade numerous investigations highlighting the weight saving potential of composite materials have resulted in the steady incremental use of composites in industries. Composite materials offer greater tailoring capabilities and higher strength and stiffness to weight ratios than their metal counterparts. In particular, the superior tailoring potential of composites stems from the separation of structural (e.g. geometry) and material (e.g. fibre orientation) degrees of freedoms (D.O.Fs) in laminates, something that is not possible with isotropic materials.

Structural optimisation has played a pivotal role in demonstrating the tailoring capabilities offered by composite materials [1]. However, the large number of design D.O.Fs providing composite structures with great tailorability also results in a complex search space including both continuous and integer design variables [2], as well as new failure criteria. The size and shape optimisation methods previously developed for metals structure [3, 4] consequently proved to be insufficiently equipped to satisfactorily optimise composite structures. As a result, the optimisation of composite structure is often limited to a small design subspace in which laminates effectively behave like isotropic metals (i.e. quasi-isotropic laminates, also referred to as black metal).

The complex design space associated with composite structures has encouraged the development of new optimisation methods [5] and parameterisations [6]. Wherever metals or composites are used, structural

---

<sup>1</sup>Post-doctoral Researcher, Bristol Composite Insitute (ACCIS), University of Bristol, BS8 1TR, United Kingdom. Corresponding author E-mail address: terence.macquart@bristol.ac.uk

<sup>2</sup>PhD Candidate, Bristol Composite Insitute (ACCIS), University of Bristol, BS8 1TR, United Kingdom

<sup>3</sup>PhD Candidate, ONERA - The French Aerospace Lab, F-92322 Chatillon, France

<sup>4</sup>Lecturer in Composite Structures and EPSRC Research Fellow, Bristol Composite Insitute (ACCIS), University of Bristol, BS8 1TR, United Kingdom

<sup>5</sup>Professor in Lightweight Structures, Bristol Composite Insitute (ACCIS), University of Bristol, BS8 1TR, United Kingdom

stiffness properties must be calculated before performance can be assessed. Classical laminate theory (CLT) provides a straightforward means of determining the stiffness properties of a composite laminate based on its stacking sequence (i.e. assembly of plies). Although simple, a number of variables directly proportional to the number of plies (e.g. ply orientation and thickness) is required to encompass the entire design space of a laminate whilst using CLT. By contrast, lamination parameters provide a compact and continuous parameterisation of a laminate's design space [7]. By taking advantage of material invariants, a set of twelve lamination parameters and a thickness variable are sufficient to express the stiffness properties of a laminate, as illustrated in Figure 1. Meaning that thirteen parameters can replace the  $N$  variables needed by CLT to evaluate the stiffness properties of an  $N$ -ply laminate. Even more importantly, employing lamination parameters as design variables reformulates composite optimisations as continuous problems compatible with the use of computationally efficient gradient based optimisers.

Although many researchers have recognised the advantages of using lamination parameters [8, 9, 10, 11], some crucial challenges associated with this approach remain unsolved. The lamination parameter space is a  $12^{th}$ -dimensional hypercube, with each dimension bound in  $[-1, 1]$  by the very definition of lamination parameters. Additionally, a combination of mathematical expressions, referred to as feasibility constraints, are necessary to satisfy the interdependent geometrical and trigonometrical relationships between individual lamination parameters. The application of these constraints effectively restricts lamination parameters to lie within a convex subspace of the initial hypercube[12]. An analogous 3D representation of this subspace is depicted in Figure 2A. Lamination parameters within the feasible design space are physically meaningful and correspond to realistic stiffness properties. Conversely, values outside the feasible subspace do not correspond to physical stiffness properties and can result in non-computable structural properties (i.e. non-positive definite stiffness matrices). Non-computable solutions are to be avoided for successful optimisation, and consequently a considerable number of constraints must be used to satisfy the interdependent mathematical relationships between lamination parameters.

In view of its importance, defining the feasible lamination parameters design space and enforcing the corresponding feasibility constraints remains an active topic of research. While significant efforts have been dedicated to the derivation of feasibility constraints, no one, to the best of the authors' knowledge, has investigated the methods used to enforce these constraints. Accordingly, this paper focuses solely on the enforcement of feasibility constraints.

Let us consider the shell structure illustrated in Figure 1, divided into eight regions, each of constant stiffness property. Using lamination parameters, only thirteen design variables per region, or 104 in total, are needed to describe the entire shell structural properties. The number of feasibility constraints necessary to ensure that physically meaningful solutions are retrieved is expressed as  $8 \times N_{constr}$  where  $N_{constr}$  is the number of constraints per region. Although different formulations of these constraints have been proposed in the literature,  $N_{constr}$  is typically expressed as either a set of non-linear constraints for orthotropic materials[7] (i.e. generally 22 constraints) or more generally as tens of thousand of linear constraints[13]. The total number of constraints for the optimisation of this simple structure, therefore, lies between 168 and 80000+. As previously explained, these constraints must be strictly enforced during the optimisation to obtain feasible lamination parameters. Handling that many constraints through penalty or interior point optimisation methods can, however, have a deteriorating effect on the optimiser's performance. In spite of this issue, alternative ways of dealing with feasibility constraints have not yet been investigated in the field of composites optimisation. An innovative approach to this problem is presented in this paper.



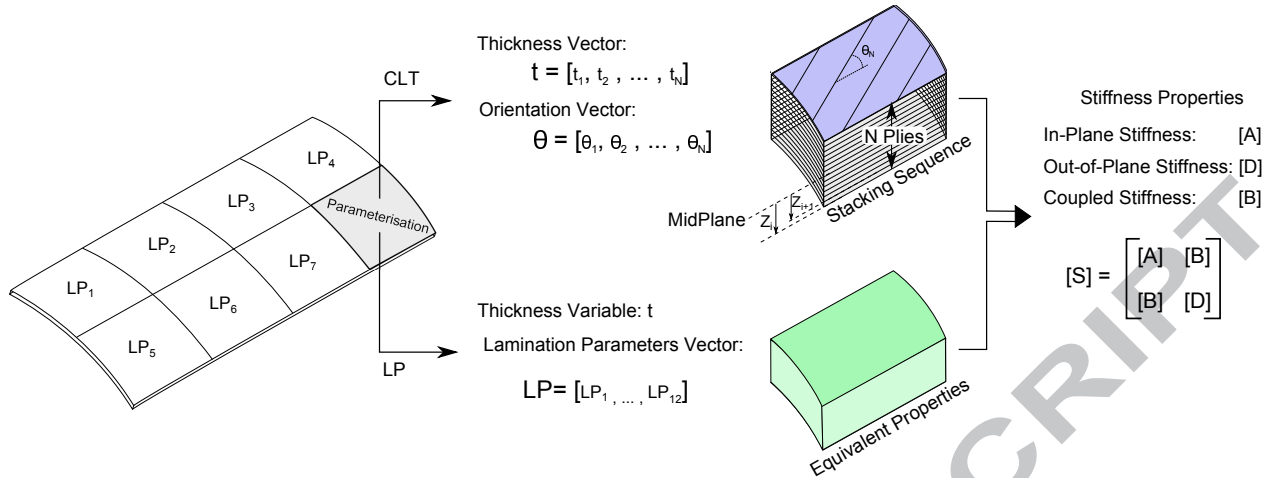


Fig. 1 Composite structure parameterisations based on classical laminate theory (CLT) and lamination parameters (LP)

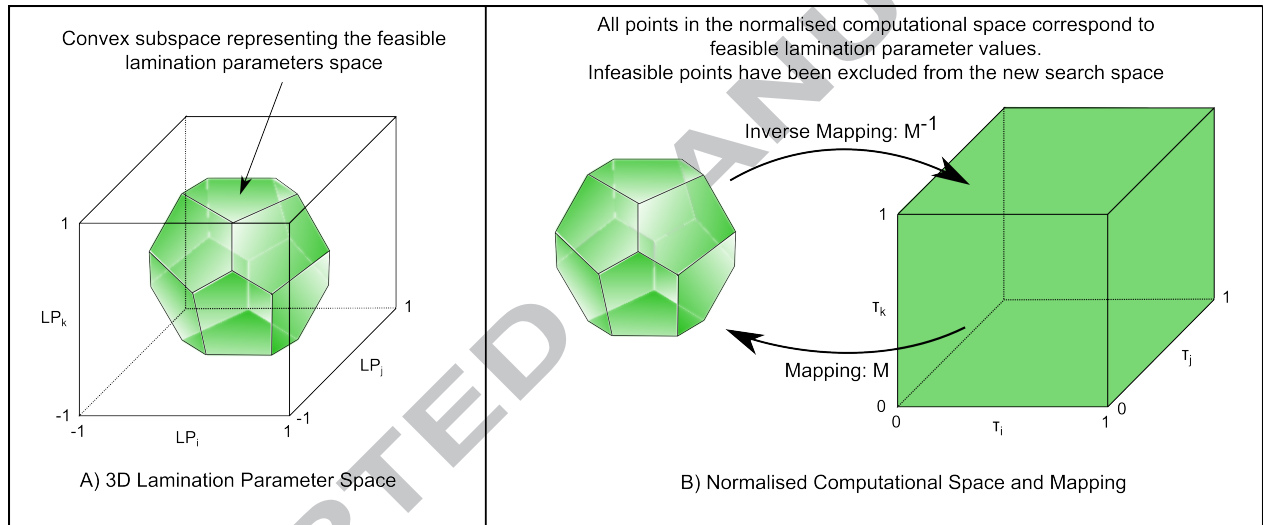


Fig. 2 Feasible mapping ideology

The novelty of this work revolves around the application of maps to the lamination parameters feasible space as a means to facilitate and speed-up the optimisation of composite structures. Our aim is to demonstrate, with proof-of-concepts, that maps can be derived and successfully applied for composite laminate optimisation. To this end, we propose a procedure for computing bijective maps between a normalised computational space and the lamination parameters feasible design space, as illustrated in Figure 2B. As depicted in this figure, the proposed maps inherently include feasibility constraints, hence unburdening the optimiser. Employing these maps simplifies the optimisation loop as shown, through comparison, in Figure 3. As seen in this figure, the feasibility constraints denoted by  $\mathbf{g}_2$  are removed from the optimisation process and replaced by normalised design variables  $\boldsymbol{\tau}$  and the map  $M$  converting these variables into feasible lamination parameters. Conveniently, with this new approach the  $\mathbf{g}_2$  feasibility constraints that previously needed to be checked repeatedly during each optimisation step become redundant. Instead, the feasibility constraints are employed in a pre-optimisation step to compute the map  $M$ . Computational improvements are expected to originate from switching the enforcement of feasibility constraints from an explicit approach to an implicit method based on maps.

The rest of this paper is structured as follows. Conventional definitions of the lamination parameters and their feasibility constraint boundaries are presented in Section 2, whilst the proposed maps are presented

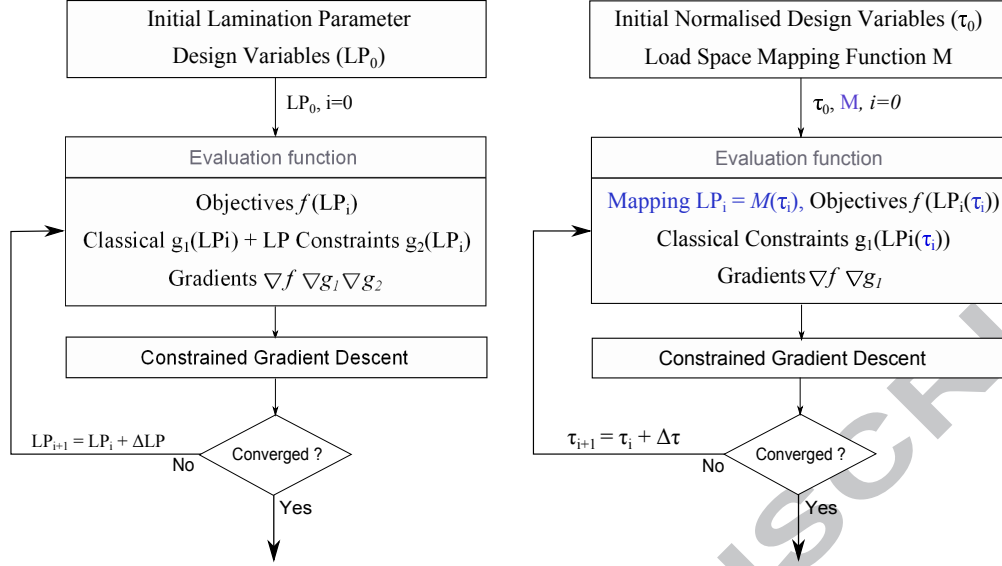


Fig. 3 Conventional and mapped optimisation loop

in Section 3. Next, Section 4 demonstrates their application through benchmark optimisation problems. Section 5 concludes the article with a discussion on the mapping methodologies and their potential benefits.

## 2. Lamination Parameters

Initially proposed in 1968 by Tsai *et al.*[14], the concept of lamination parameters is briefly introduced in this section. Employing lamination parameters provides a compact and continuous parametrisation for composite laminates, a convenient alternative to stacking sequences. Tsai and Hahn[15] showed that the stress/strain stiffness values of a ply oriented at an angle  $\theta$  can be expressed as linear combinations of material invariants  $U_i$ , with  $i = 1, \dots, N$ , and trigonometric functions as illustrated in Figure 4. Once these are combined with CLT, the expressions for in-plane  $[A]$ , out-of-plane  $[D]$  and coupled  $[B]$  stiffness properties of composite laminates are greatly simplified. Let us consider the  $[A], [B], [D]$  stiffness matrices in the expression

$$\begin{bmatrix} \mathbf{N} \\ \mathbf{M} \end{bmatrix} = \begin{bmatrix} [A] & [B] \\ [B] & [D] \end{bmatrix} \begin{bmatrix} \boldsymbol{\epsilon}_0 \\ \boldsymbol{\kappa} \end{bmatrix}, \quad (1)$$

in which  $\mathbf{N}$  and  $\mathbf{M}$  are the force and moment resultants per unit width, and  $\boldsymbol{\epsilon}_0$  and  $\boldsymbol{\kappa}$  are the laminate's mid-plane strains and curvatures, respectively. The in-plane  $[A]$ , out-of-plane  $[D]$  and coupled  $[B]$  stiffness matrices are obtained using CLT such that

$$[A] = \sum_{i=1}^N [\bar{Q}]_i (Z_i - Z_{i-1}), \quad [D] = \frac{1}{3} \sum_{i=1}^N [\bar{Q}]_i (Z_i^3 - Z_{i-1}^3), \quad [B] = \frac{1}{2} \sum_{i=1}^N [\bar{Q}]_i (Z_i^2 - Z_{i-1}^2), \quad (2)$$

where the location of the interfaces between plies are given by  $Z_i$  and  $Z_{i-1}$ . Now substituting the stiffness properties of plies  $[\bar{Q}]_i$  by their equivalent material invariants and trigonometric functions one can rewrite the in-plane stiffness matrix as

$$[A] = \sum_{i=1}^N ([T_0]_i + [T_1]_i \cos(2\theta_i) + [T_2]_i \cos(4\theta_i) + [T_3]_i \sin(2\theta_i) + [T_4]_i \sin(4\theta_i)) (Z_i - Z_{i-1}), \quad (3)$$

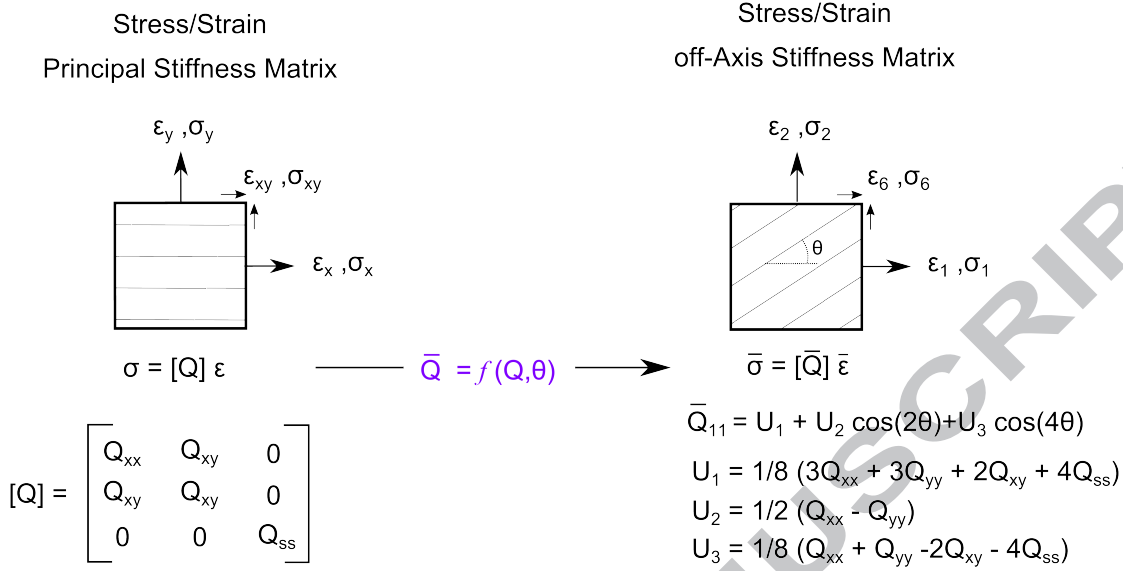


**Fig. 4** Relationship between principal and off-axis stress/strain stiffness for a single ply

in which the material invariants  $U_i$  are regrouped into the invariant matrices  $[T_0]$ ,  $[T_1]$ ,  $[T_2]$ ,  $[T_3]$  and  $[T_4]$ . The significant reduction of design variables using lamination parameters becomes evident as we rearrange Eq. (3) for a laminate made of a single material. In this case the material invariants are independent of plies and can be moved outside the summation as follows

$$[A] = [T_0] \sum_{i=1}^N (Z_i - Z_{i-1}) + [T_1] \sum_{i=1}^N \cos(2\theta_i) (Z_i - Z_{i-1}) + [T_2] \sum_{i=1}^N \cos(4\theta_i) (Z_i - Z_{i-1}) + [T_3] \sum_{i=1}^N \sin(2\theta_i) (Z_i - Z_{i-1}) + [T_4] \sum_{i=1}^N \sin(4\theta_i) (Z_i - Z_{i-1}), \quad (4)$$

meaning that  $[A]$ , after defining the in-plane lamination parameters as

$$\begin{aligned} V_1^A &= \frac{1}{h} \sum_{i=1}^N \cos(2\theta_i) (Z_i - Z_{i-1}), & V_2^A &= \frac{1}{h} \sum_{i=1}^N \cos(4\theta_i) (Z_i - Z_{i-1}) \\ V_3^A &= \frac{1}{h} \sum_{i=1}^N \sin(2\theta_i) (Z_i - Z_{i-1}), & V_4^A &= \frac{1}{h} \sum_{i=1}^N \sin(4\theta_i) (Z_i - Z_{i-1}) \end{aligned}, \quad (5)$$

can be expressed as a linear combination of lamination parameters and material invariant matrices

$$[A] = h ([T_0] + [T_1]V_1^A + [T_2]V_2^A + [T_3]V_3^A + [T_4]V_4^A), \quad (6)$$

with  $h$  being the laminate thickness.

By definition, lamination parameters are weighted averages of trigonometric functions depending on the position, thickness and orientation of each ply, hence only five variables (i.e. one thickness and four lamination parameters) are required to compute the in-plane stiffness matrix. Similar expressions to Eq. (6) can be derived for the out-of-plane and coupled stiffness matrices. These equations are at the core of composite optimisation based on lamination parameters. By bypassing the CLT requirement for stacking sequences, it becomes possible to optimise laminate stiffness properties directly by means of a small set of lamination

parameters as design variables (e.g. using Eq (6) for in-plane stiffness). Most importantly, composite optimisation problems formulated with lamination parameters are continuous, enabling the use of fast gradient based optimisers.

In general, twelve lamination parameters and one thickness variable are sufficient to describe any laminate. Similarly to the  $[A]$ ,  $[B]$  and  $[D]$  stiffness matrices, lamination parameters are divided into three types corresponding to in-plane, coupled and out-of-plane structural responses. The lamination parameters notation used in this study is as follows

$$\mathbf{LP} = [V_1^A, V_2^A, V_3^A, V_4^A, V_1^B, V_2^B, V_3^B, V_4^B, V_1^D, V_2^D, V_3^D, V_4^D]^T \quad (7)$$

where,  $\mathbf{LP}$  is a vector of 12 parameters and the lamination parameters related to the laminate in-plane, out-of-plane and coupled stiffness coefficients are respectively denoted by  $V_i^A$ ,  $V_i^D$  and  $V_i^B$  with  $i = 1, 2, 3, 4$ . Lamination parameters for an N-ply laminate are calculated as per Table 1. For further details on lamination parameters the reader is referred to Gurdal *et al.* [16].

**Table 1** Lamination parameters definition,  $\theta \in [-\pi/2, \pi/2]$

In-plane	Coupled	Out-of-Plane
$V_1^A = \frac{1}{h} \sum_{i=1}^N (Z_i - Z_{i-1}) \cos(2\theta_i)$	$V_1^B = \frac{2}{h^2} \sum_{i=1}^N (Z_i^2 - Z_{i-1}^2) \cos(2\theta_i)$	$V_1^D = \frac{4}{h^3} \sum_{i=1}^N (Z_i^3 - Z_{i-1}^3) \cos(2\theta_i)$
$V_2^A = \frac{1}{h} \sum_{i=1}^N (Z_i - Z_{i-1}) \cos(4\theta_i)$	$V_2^B = \frac{2}{h^2} \sum_{i=1}^N (Z_i^2 - Z_{i-1}^2) \cos(4\theta_i)$	$V_2^D = \frac{4}{h^3} \sum_{i=1}^N (Z_i^3 - Z_{i-1}^3) \cos(4\theta_i)$
$V_3^A = \frac{1}{h} \sum_{i=1}^N (Z_i - Z_{i-1}) \sin(2\theta_i)$	$V_3^B = \frac{2}{h^2} \sum_{i=1}^N (Z_i^2 - Z_{i-1}^2) \sin(2\theta_i)$	$V_3^D = \frac{4}{h^3} \sum_{i=1}^N (Z_i^3 - Z_{i-1}^3) \sin(2\theta_i)$
$V_4^A = \frac{1}{h} \sum_{i=1}^N (Z_i - Z_{i-1}) \sin(4\theta_i)$	$V_4^B = \frac{2}{h^2} \sum_{i=1}^N (Z_i^2 - Z_{i-1}^2) \sin(4\theta_i)$	$V_4^D = \frac{4}{h^3} \sum_{i=1}^N (Z_i^3 - Z_{i-1}^3) \sin(4\theta_i)$

### 2.1. Lamination Parameters Feasible Space

Lamination parameters are geometric and trigonometric functions of plies and are consequently interdependent. When using lamination parameters as design variables it is, therefore, crucial to ensure that the coupling constraints between individual parameters are satisfied. That is, to ensure that lamination parameters can be matched to a realistic structural properties.

Consider the following example in which the first and third in-plane lamination parameters  $V_1^A$  and  $V_3^A$  are employed as design variables. The feasible design space is, in this case, intuitively given by the relationship between  $\cos(\theta)$  and  $\sin(\theta)$  that entails

$$[V_1^A]^2 + [V_3^A]^2 \leq 1, \quad (8)$$

as illustrated in Figure 5. A set of lamination parameters  $V_1^A$  and  $V_3^A$  defined outside this circle does not correspond to a physically possible stacking sequence. When optimising lamination parameters we must, therefore, ensure that Eq. (8) remains satisfied. However, lamination parameters themselves can vary individually between  $[-1, 1]$ , it is hence necessary to add Eq. (8) as a constraint during optimisation or automated design procedures. Such a simple two dimensional example demonstrates the importance of feasibility constraints. Nevertheless, accounting for all of the constraints between the twelve lamination parameters is not a trivial task. The exact boundary of the 12-dimensional feasible design space remains, as a matter of fact, unknown.

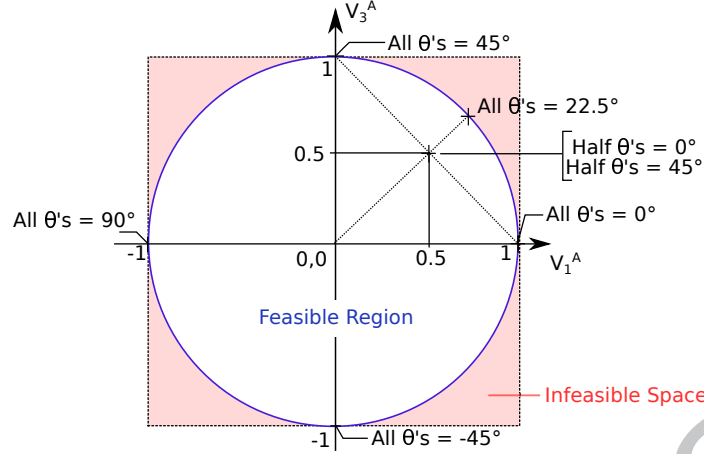


Fig. 5 Two dimensional feasibility constraints between  $V_1^A$  and  $V_3^A$

Two types of approach have been used in the literature in order to derive feasibility constraints for the lamination parameter space, these are either analytical or numerical. Numerical feasibility constraints have been derived using convex hulls. Since it has been proven that the feasible lamination parameter space is convex[12], numerical methods are based on the automated generation of lamination parameters as a means to identify the smallest convex hull regrouping all feasible solutions[13]. Employing the numerical approach proposed by Bloomfield *et al.* [13] results in a large number (e.g. tens of thousand) of hyperplane constraints describing the convex hull geometry. In contrast to numerical approaches, the analytical derivation of feasibility constraints leads to a compact description of the lamination parameters space boundaries[17, 7]. The 22 non-linear constraints summarised in Eq. (9) to (15) form a set which provides a necessary yet incomplete representation of the feasible design space since some constraints involving the coupled lamination parameters (i.e.  $V_i^B$ ) remain unknown to date. These feasibility constraints are therefore used as starting point to evaluate the proposed maps for symmetric laminates only (i.e.  $V_i^B = 0$  for  $i = 1, 2, 3, 4$ ).

$$[V_1^j]^2 + [V_3^j]^2 \leq 1, \quad (9)$$

$$2[V_1^j]^2 - V_2^j \leq 1, \quad (10)$$

$$2(1 + V_2^j)[V_3^j]^2 - 4V_1^j V_3^j V_4^j + [V_4^j]^2 - (V_2^j - 2[V_1^j]^2 + 1)(1 - V_2^j) \leq 0, \quad (11)$$

where  $j = A, D$ . Additional relationships couple together the in- and out-of-plane properties, as well as relate them to the coupling terms

$$\frac{1}{4}(V_i^A + 1)^3 - 1 \leq V_i^D \leq \frac{1}{4}(V_i^A - 1)^3 + 1, \quad (12)$$

$$4(V_i^A + 1)(V_i^D + 1) \geq (V_i^A + 1)^4 + 3[V_i^B]^2, \quad (13)$$

$$4(V_i^A - 1)(V_i^D - 1) \geq (V_i^A - 1)^4 + 3[V_i^B]^2, \quad (14)$$

where  $i = 1, 2, 3, 4$ . Wu *et al.*[7] also recently showed that

$$5 (V_1^A - V_1^D)^2 - 2 (1 + V_2^A - 2[V_1^A]^2) \leq 0, \quad (15)$$

is an important, and seemingly little known, inequality constraints for lamination parameters feasibility. The addition of these non-linear constraints, which must be strictly enforced for each set of lamination parameters, during optimisation can negatively impact the performance of optimisers. In the following section we propose two mapping strategies that greatly simplify the enforcement of feasibility constraints within optimisation procedures.

### 3. Feasibility Maps

The novelty of this work revolves around the derivation and application of maps to the feasible lamination parameters space. The idea is to replace lamination parameters by normalised design variables which, once mapped, correspond to feasible lamination parameters. That is, each point in the normalised computational space is associated with a single point in the feasible lamination parameters space. In other words, the proposed feasibility maps inherently exclude the infeasible region of the lamination parameter space, thereby, ensuring that the remaining space solely contain feasible solutions.

Two mapping strategies are investigated in this paper. First, an intuitive and straightforward map based on the sequential application of linear scaling is introduced. Second, a more generic map based on the use of B-splines is proposed. As a proof of concept, a limited number of constraints and lamination parameters are employed in this paper in order to demonstrate the viability of the proposed maps. Two and three dimensional maps of the  $V_1^A$ ,  $V_2^A$  and  $V_3^A$  lamination parameters with respect to the constraints given in Eqs. (9) to (11) are now introduced.

#### 3.1. Linear Scaling Map

A simple map based on the sequential application of linear scaling is presented in this section. Before further details are given regarding the mapping, some points of clarification on the nomenclature used are given.

- The lamination parameter space refers to a  $N$ -dimensional hypercube defined by the individual bounds of each parameters (i.e.  $[-1, 1]$ ) and upon which constraints must be applied to identify its feasible subspace dimension and shape. Additionally, this space varies as a function of the number of lamination parameter design variables used for optimisation, in the most general case  $N = 12$ .
- The 'computational space' refers to a  $N$ -dimensional hypercube. In the case of linear scaling this hypercube has the same dimensionality as the lamination parameters space. The computational space is defined upon the base formed by vectors  $\beta_i^j$ . All points within the computational space correspond to feasible lamination parameters as illustrated in Figure 6 for a two-dimensional mapping.

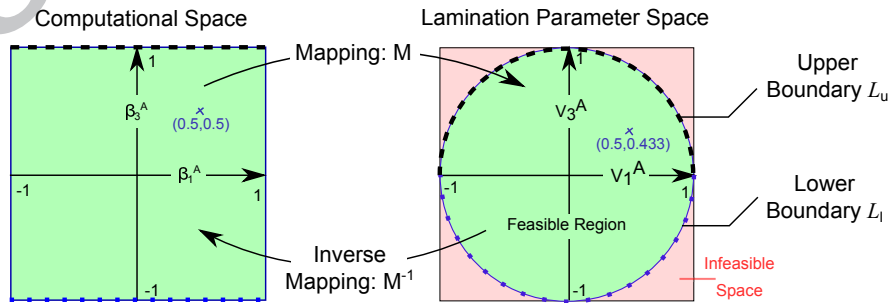


Fig. 6 Lamination parameters and computational space, 2D example

The general linear scaling formula is

$$V_i^j = \frac{1}{2} (L_u(i, j) + L_l(i, j)) + \frac{1}{2} (L_u(i, j) - L_l(i, j)) \beta_i^j, \quad (16)$$

where  $V_i^j$  and  $\beta_i^j$ , with  $i = 1, 2, 3, 4$ , and  $j = A, B, D$ , respectively denote the lamination parameters and computational space normalised variables. The normalised variables  $\beta_i^j$  are bound between  $[-1, 1]$  corresponding to the lamination parameter values of  $[L_l(i, j), L_u(i, j)]$ .

For the sake of clarity, we start with a linear scaling example from which the three normalised variables  $\beta_1^A$ ,  $\beta_2^A$  and  $\beta_3^A$  are mapped to their corresponding feasible lamination parameters  $V_1^A$ ,  $V_2^A$  and  $V_3^A$ . In this case, we only need to consider the constraints given by Eqs. (9), (10) and (11), all other lamination parameters are assumed to be zero.

The lamination parameter  $V_2^A$  is chosen as starting point and remains unscaled such that

$$1^{st} \text{ Scaling step: } V_2^A = \beta_2^A. \quad (17)$$

The second step consists of scaling  $V_1^A$  with respect to  $V_2^A$  based on the feasibility constraints given by Eq. (10). The upper and lower feasibility bounds imposed onto  $V_1^A$  by this constraint are easily found by rewriting the latter equation as

$$\underbrace{-\sqrt{0.5(V_2^A + 1)}}_{L_l} \leq V_1^A \leq \underbrace{\sqrt{0.5(V_2^A + 1)}}_{L_u}. \quad (18)$$

The upper and lower bounds found for  $V_1^A$  are then used in Eq. (16) to obtain the value of  $V_1^A$  as follows

$$2^{nd} \text{ Scaling step: } V_1^A = \beta_1^A \sqrt{0.5(V_2^A + 1)}. \quad (19)$$

Next, the constraints employed in order to calculate  $V_3^A$  with respect to  $V_1^A$  and  $V_2^A$  are given by Eqs. (9) and (11) assuming that  $V_4^A = 0$ . Rewriting Eq. (9) to obtain the feasibility boundaries of  $V_3^A$  we have

$$-\sqrt{1 - [V_1^A]^2} \leq V_3^A \leq \sqrt{1 - [V_1^A]^2}, \quad (20)$$

and by solving the quadratic equation associated with the equality corresponding to Eq. 11 and rearranging we obtain

$$(V_3^A)^2 \leq \frac{1}{2(1 + V_2^A)} (V_2^A - 2(V_1^A)^2 + 1)(1 - V_2^A). \quad (21)$$

The maximum and minimum bounds for  $V_3^A$  are given by Eqs. (20) and (21), and the scaled value of  $V_3^A$  is then evaluated as

$$3^{rd} \text{ Scaling step: } V_3^A = \frac{1}{2} (V_{3u}^A + V_{3l}^A) + \frac{1}{2} (V_{3u}^A - V_{3l}^A) \beta_3^A, \quad (22)$$

with

$$V_{3l}^A = \max \left\{ -\sqrt{1 - [V_1^A]^2}, \quad -\sqrt{\frac{1}{2(1+V_2^A)} (V_2^A - 2(V_1^A)^2 + 1)(1 - V_2^A)} \right\} \quad (23)$$

and

$$V_{3u}^A = \min \left\{ \sqrt{1 - [V_1^A]^2}, \quad \sqrt{\frac{1}{2(1+V_2^A)} (V_2^A - 2(V_1^A)^2 + 1)(1 - V_2^A)} \right\}. \quad (24)$$

The application of linear scaling maps including more lamination parameters follows the exact same procedure as the one just presented. A first parameter is scaled, then a second with respect to the first and so on until all  $\beta_i^j$  values are converted into feasible lamination parameters. Note that while this mapping in higher dimension is somewhat cumbersome, its application is simple and, most importantly, computationally cheap. It should be noted that for most lamination parameters, the feasibility boundaries are formed by multiple constraints acting simultaneously. In such cases, the smallest feasible space boundaries should be used for upper and lower bounds as in Eq. (22).

### 3.2. B-Spline Map

B-Splines and non-uniform rational B-spline (NURBS) have been widely used in CAD systems for representing complex geometries with a relatively small number of design variables. In this section, B-splines are used to approximate the feasible lamination parameter space and provide a mapping between the spline design variables and feasible lamination parameters. While other generic methods could be employed to generate this feasibility map, B-splines are preferred due to their ease of implementation, simple mathematical formulation and convex hull property. Ensuring the convexity of the approximated space is important because even marginally infeasible lamination parameters can result in a failed analysis. For the sake of simplicity, yet without loss of generality, linear B-splines are used in this study. As done previously, the nomenclature used for the B-spline mapping is:

- The B-spline computational space also refers to a  $N$ -dimensional hypercube. In this case the hypercube sides are defined between  $[0, 1]$  and spline variables  $\tau$  are used to navigate this space. As for the sequential linear mapping, all points within the computational space correspond to feasible lamination parameters as illustrated by the two-dimensional example in Figure 7.

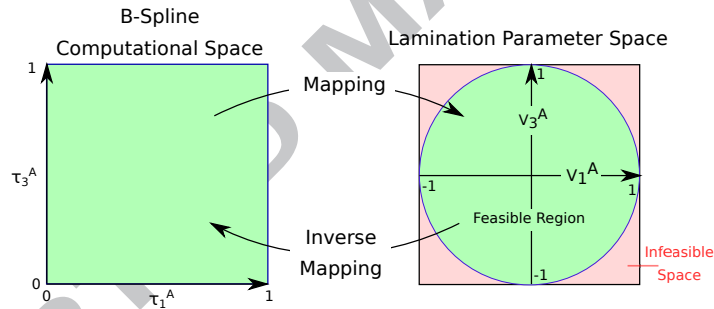


Fig. 7 Lamination parameter space and B-spline computational space, 2D example

The two-dimensional space shown in Figure 7 is approximated using a linear spline surface. The proposed mapping procedure is presented in Figure 8. First, the feasible design space boundaries are determined, either analytically or numerically. Then the feasibility boundaries are used to create a mesh spanning the entire feasible design space in step 1. The mesh points generated, combined with the spline basis functions, are then used in step 2 as control points in order to compute the spline map between the computational space and the lamination parameter space. After completion of step 2, points within the feasible design space can be obtained by substituting the spline variables  $\tau$  in the surface equation  $C$ .



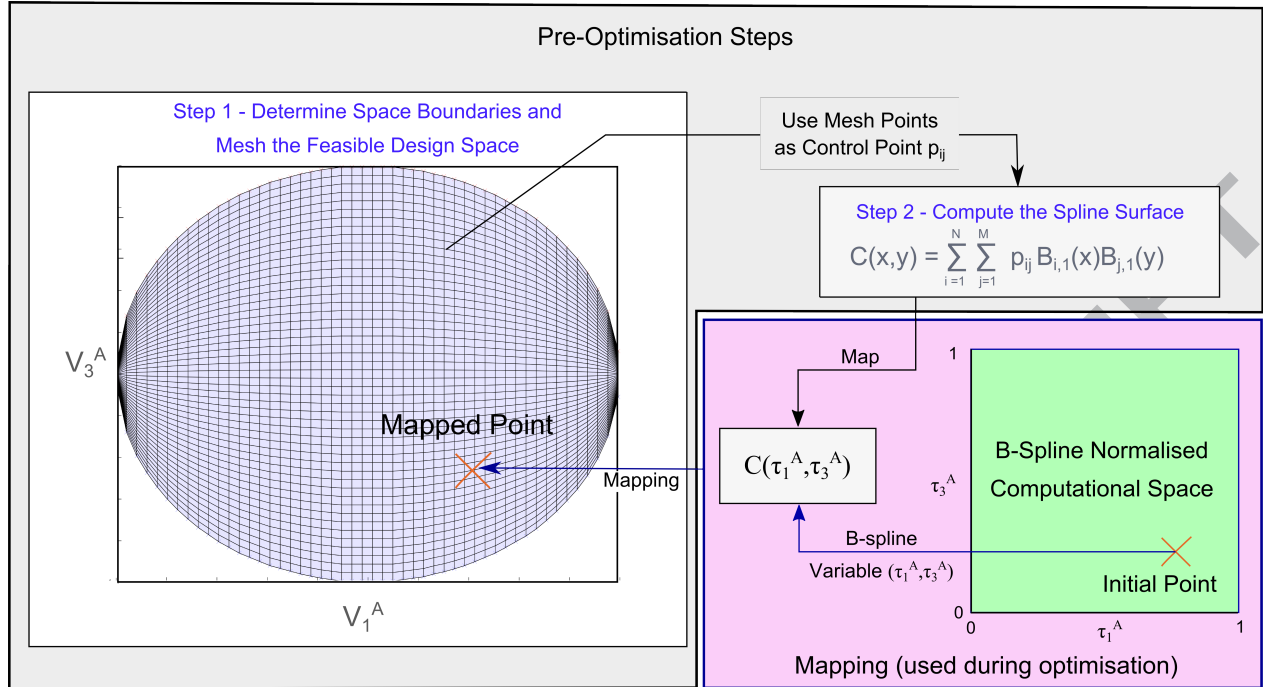


Fig. 8 Spline mapping procedure

In contrast to the linear scaling map presented in Section 3.1, the B-spline map is derived numerically. That is, the feasibility boundary constraints do not have to be manipulated in order to create the map. The determination of boundaries, the meshing and, the spline surface computation can all be automated. However, the computational cost for higher dimensional problems is rather expensive for this approach. That is, in part, because a uniform radial basis is used in this study. A mapping based instead on NURBS could greatly reduce the number of mesh point required to accurately map the feasible lamination parameter space.

#### 4. Verification and Application

The behaviour of maps proposed in Section 3 is now numerically verified. Heuristic mapping examples are used to ensure that only feasible solutions are generated whilst using the maps. Maps are then used to solve benchmark optimisation problems and their effects on the optimal path and the space convexity are investigated.

##### 4.1. Linear Scaling Map Verification

The lamination parameter design space obtained after applying the linear map on randomly generated points in the computational space for 2D and 3D cases are presented in Figures 9 and 10, respectively. Figure 9 shows the linear mapping of  $V_1^A$  and  $V_3^A$  while considering constraints given by Eqs. (9) and (11) and assuming  $V_2^A = V_4^A = 0$ . As seen in this figure, random points initially generated in the  $[-1, 1]$  two dimensional computational space are all mapped onto the feasible region domain. Similarly, the three dimensional mapping including  $V_1^A$ ,  $V_2^A$  and,  $V_3^A$  and considering constraints given by Eqs. (9) to (11) is shown in Figure 10.

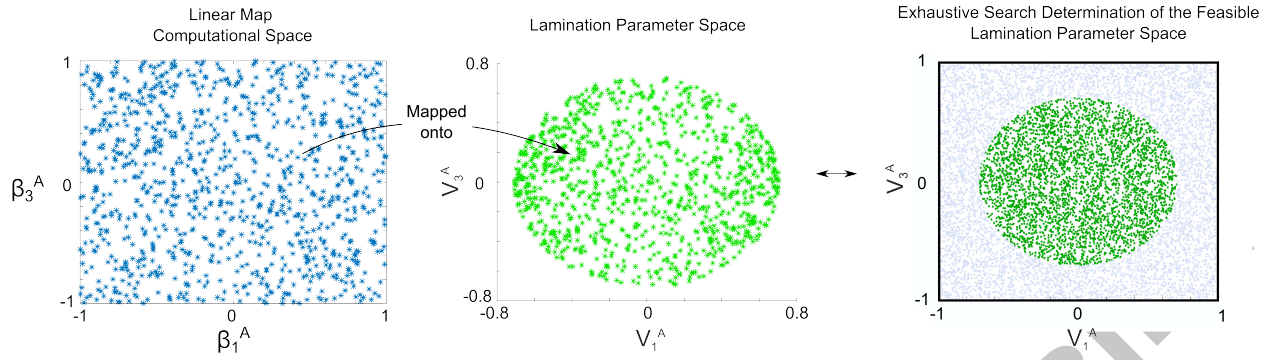


Fig. 9 2D linear map verification - 1000 points

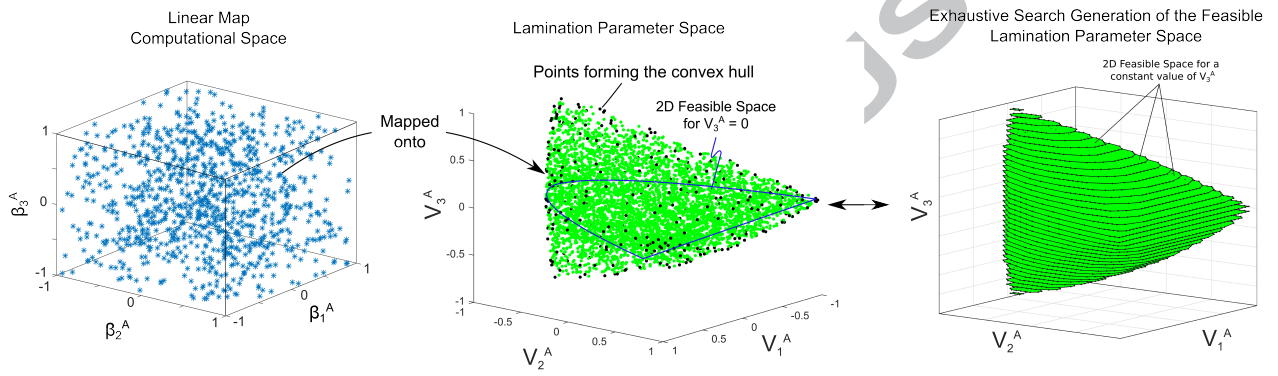


Fig. 10 3D linear map verification - 1000 points

#### 4.2. B-spline Map Verification

Similarly to the verification carried out for the linear maps, the B-spline maps for the 2D and 3D cases are shown in Figures 11 and 12, respectively. As observed in these figures, the B-spline two and three dimensional maps are similar to the ones obtained with the linear scaling maps. In both cases, all lamination parameter constraints considered during the mapping are automatically enforced during the mapping between the computational space and the lamination parameters space.

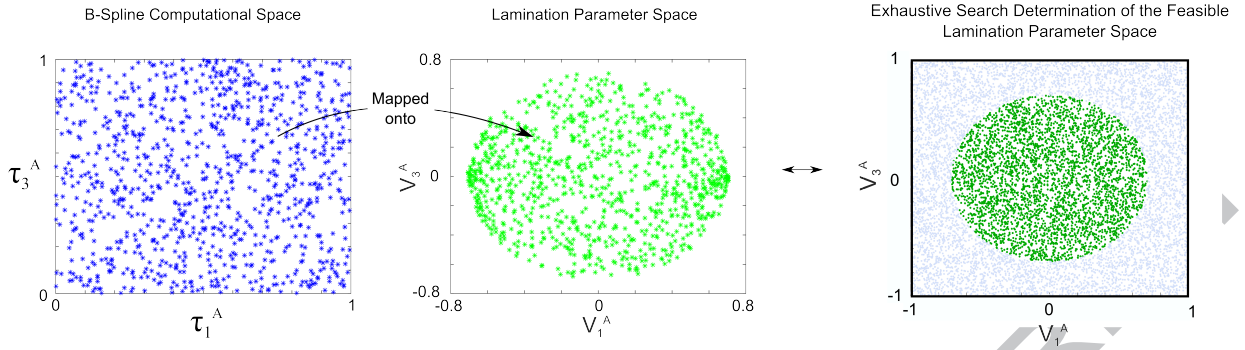


Fig. 11 2D B-spline map verification - 1000 points

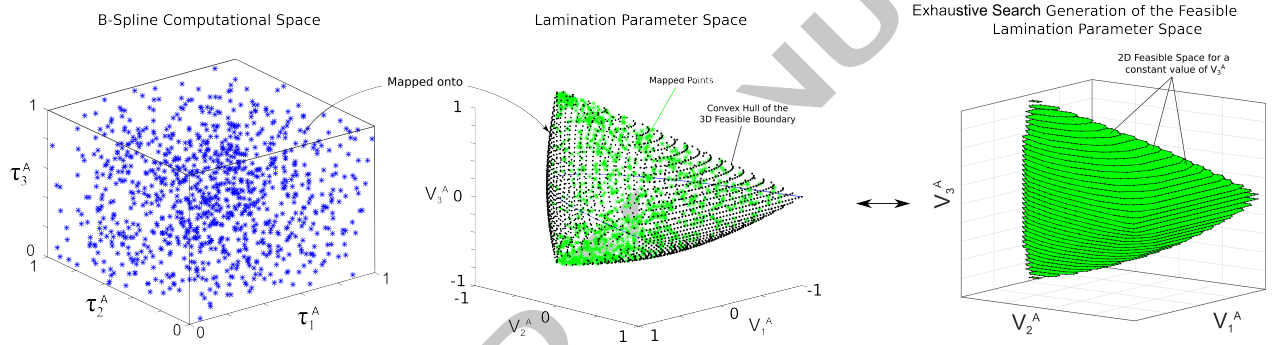


Fig. 12 3D B-spline map verification - 1000 points

#### 4.3. Mapping Applied to a Benchmark Optimisation Problem

In this section the Rosenbrock function, often used to benchmark optimisers, is employed to assess convergence with and without maps. The two dimensional Rosenbrock optimisation problem is defined as

$$f = 100(V_3^A - (V_1^A)^2) + (V_1^A - 1)^2, \quad (25)$$

	Classic	Linear Mapping	Spline Mapping
min	$f(V_1^A, V_3^A)$	$f(V_1^A, V_3^A)$	$f(V_1^A, V_3^A)$
with:		$V_1^A = V_1^A(\beta_1^A, \beta_3^A)$ $V_3^A = V_3^A(\beta_1^A, \beta_3^A)$	$V_1^A = V_1^A(\tau_1^A, \tau_3^A)$ $V_3^A = V_3^A(\tau_1^A, \tau_3^A)$
subject to:	$-1 \leq V_1^A \leq 1$ $-1 \leq V_3^A \leq 1$ Eq. (9 – 11)	$-1 \leq \beta_1^A \leq 1$ $-1 \leq \beta_3^A \leq 1$	$0 \leq \tau_1^A \leq 1$ $0 \leq \tau_3^A \leq 1$

Employing a mapping between the computational space and the feasible lamination parameter space within an optimisation loop alters the optimiser’s design space. As such, it is judicious to ensure that the mapped design space, as seen by the optimiser, remains smooth. As done previously, the mappings are obtained for  $V_1^A$  and  $V_3^A$  while only considering the lamination parameter constraints (9) to (11). The various design spaces obtained with and without mapping are shown in Figure 13. First, the original unconstrained and unmapped design space is shown in Figure 13a while Figure 13b shows the constrained design space. The normalised design space corresponding to the linear scaling map and is shown in Figure 13c. As seen in this figure, any  $[-1, 1]$  combination of the mapped design variables  $\beta_1^A$  and  $\beta_3^A$  corresponds to a feasible point. This is made particularly obvious when comparing the range of colours between Figures 13b and 13c. A graphical way to think about the mapping, though not strictly correct, is to imagine the constrained circular design spaces shown in Figures 13b being stretched into a square as in Figure 13c. One can note that in comparison to the initial design space shown in Figure 13a, the mapped design space presents some irregularities toward the maximal values of  $V_1^A$  (i.e. boundaries of  $\beta_1^A$ ) at which a unique solution exists in order for constraints given by Eq. (9) to be satisfied. While this may have a negative impact on the optimiser’s performance, this edge of the feasible lamination parameter space is rarely relevant if manufacturing constraints, such as the ten-percent rule[18], are also considered during the optimisation. A similarly mapped design space, yet discretised, is obtained using the generic B-spline approach as shown in Figure 13d.

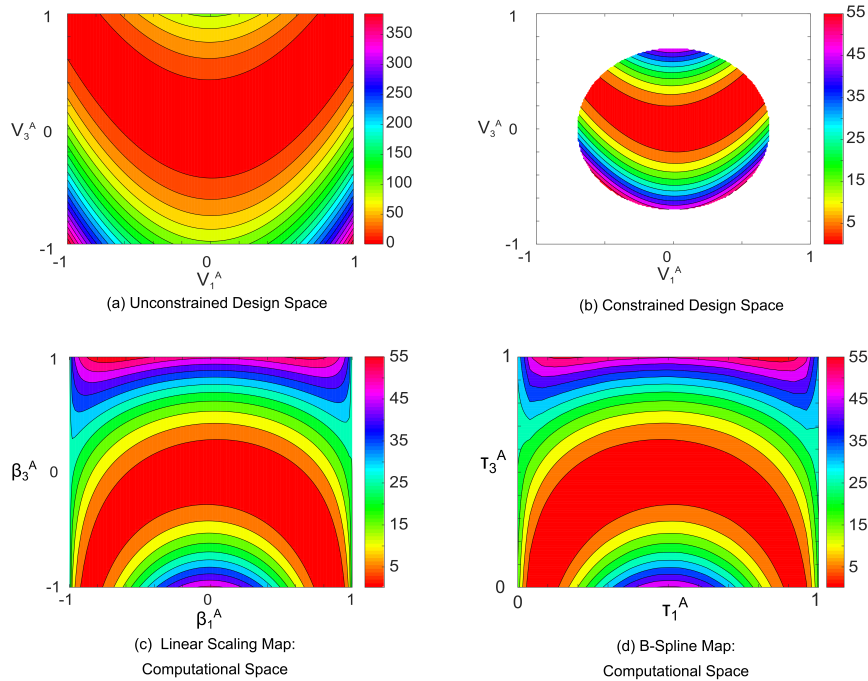


**Fig. 13** Original and mapped 2D Rosenbrock function

Optimisation runs with and without the maps are carried out using MATLAB’s FMINCON function. Results are presented in Figure 14 which shows that the optimiser reaches the optimal feasible solution, located on the design space boundary, for the classical as well as for the mapped optimisation problems. The path taken by the optimisers are, on the other hand, significantly different. The classical optimiser rapidly descends into the valley (i.e. red region) before slowly continuing the descent following the small gradient change in the valley bottom. By contrast, the first steps taken by both mapped optimisers are towards the feasible design space boundary on either side of the optimal point before converging into the valley. Removing the non-linear constraints for the mapped optimisation problem allows the optimiser to overshoot its first gradient step without being penalised, therefore reaching a near optimal design point in one step. Note

that, once on the valley bottom, the mapped optimisers expand their search range locally by moving up the valley before returning to the optimal solution. This behaviour is typical of FMINCON which allows local deviation from the optimal gradient descent path for greater robustness. Most importantly, the first steps taken by the mapped optimisers can be seen to lie exactly on the design space boundary, ensuring the feasibility of lamination parameters. These preliminary results demonstrate the potential application of lamination parameters mapping for structural optimisation. Repeated runs with various starting points, not reported here, were also found to converge to the optimal solution. In this analytical optimisation case study the optimiser speed was not investigated because of the negligible computational cost of the evaluation function and of the small number of feasibility constraints resulting in a negligible difference with the mapped optimisation.

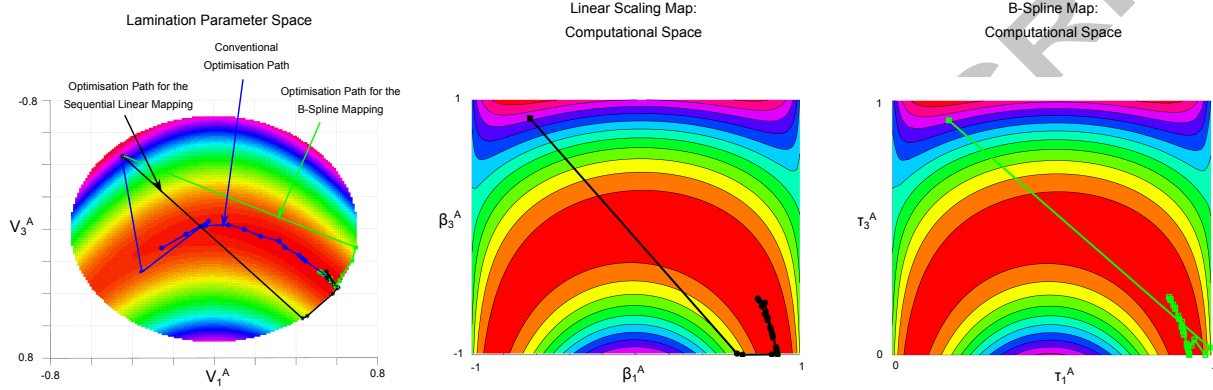


Fig. 14 Compared optimisation path between classical and mapped space of the 2D Rosenbrock function

#### 4.4. Mapping Applied to a 4D Rosenbrock Optimisation Problem

In this section the four lamination parameters  $V_1^A$ ,  $V_2^A$ ,  $V_1^D$  and  $V_2^D$  are mapped and used during the benchmark optimisation of the 4-D Rosenbrock function defined as

$$f = 100(V_2^A - [V_1^A]^2) + (V_1^A - 1)^2 + 100(V_1^D - [V_2^D]^2) + (V_2^D - 1)^2 \quad (27)$$

	Classic	Linear Mapping	Spline Mapping
min	$f(V_i^j)$	$f(V_i^j)$	$f(V_i^j)$
with:			
subject to:			
	$-1 \leq V_i^j \leq 1$ Eq. (10 – 12)	$-1 \leq \beta_i^j \leq 1$	$0 \leq \tau_i^j \leq 1$

with  $i=(1,2)$ ,  $j=(A,D)$ .

The convergence plots obtained for a single run starting at  $[-0.28933, 0.2212, -0.14156, 0.015794]$  in lamination parameter space are presented in Figure 15. Furthermore, the values for optimal design variables and fitness function corresponding to the conventional, linear and B-spline mapped optimisations are summarised in Table 2. As observed in Figure 15, the proposed mapped optimisation strategies do successfully converge

to the results obtained by means of conventional optimisation method on the original design space. However, the B-spline mapping clearly does not reach the optimal solution. This convergence issue is believed to be related to the difficulties associated with the generation of an exact 4D mesh for the feasible design space necessary to create the B-spline map. In particular, some meshing irregularities towards the optimal point  $[1, 1, 1, 1]$  located on the feasible design space boundary are likely to occur. Conversely, the linearly mapped optimisation problem converges satisfactorily. This example demonstrates the successful use of four dimensional mapping for lamination parameter optimisation.

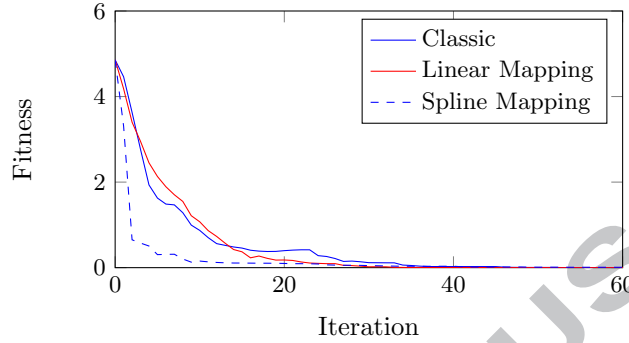


Fig. 15 Compared optimisation results between classical and mapped space of the 4D Rosenbrock function

Table 2 Optimal results for the 4D Rosenbrock optimisation runs

Optimisation	$V_1^A$	$V_2^A$	$V_1^D$	$V_2^D$	Optimal Fitness
Conventional	0.99996	0.99992	0.99996	0.99993	$2.8694 \times 10^{-9}$
Linear Map	0.99997	0.99994	0.99997	0.99994	$5.12 \times 10^{-8}$
B-Spline Map	0.93333	0.87111	0.93333	0.87111	0.0088889

#### 4.5. Mapping Applied to a Structural Optimisation Problem

As a last example the proposed 4D linear map presented in the previous section is applied to the buckling optimisation of a variable stiffness simply supported square plate, illustrated in Figure 16. The plate is assumed to be symmetric in both directions and the design variables are, therefore, only defined over a quarter of the plate as shown in Figure 16. Following our usual procedure the optimisation problem is formulated as

$$f(V_1^A, V_2^A, V_1^D, V_2^D) = \frac{1}{\text{First Plate Buckling Load}} \quad (29)$$

	Classic	Linear Mapping
min	$f(V_i^j)$	$f(V_i^j)$
with:		$V_i^j = V_i^j(\beta_1^A, \beta_2^A, \beta_1^D, \beta_2^D)$ ,
subject to:	$-1 \leq V_i^j \leq 1$	$-1 \leq \beta_i^k \leq 1$
	Eq. (10 – 12)	

(30)



with  $i=(1,2)$ ,  $j=(A,D)$ . Nine points uniformly distributed over the quarter plate are used to define point-wise properties. The value of lamination parameters over the quarter plate are then obtained using spline interpolation. Splines are used because of their convex hull properties, ensuring the lamination parameters feasibility over the whole plate if the initial nine points are feasible. MATLAB is employed to run the optimisation which wraps ABAQUS model and solver. The run time for a gradient based iteration is relatively slow and only the linear map is investigated as a result. The optimisers run until a convergence criteria based on the relative change of the fitness function is satisfied.

The optimisation results are presented in Figures 17 and 18, and summarised in Table 3. Figure 17 shows the evolution of the optimal fitness while Figure 18 highlights the similarities between the final lamination parameters distribution obtained with and without mapping. It is observed that the plate design achieved by the linear map optimisation successfully reaches the feasible design space boundary (i.e. lamination parameters close to -1 and 1) without violating any of the feasibility constraints. By contrast, the classical plate design approaches the space boundary at a much slower rate that is likely due to the effect of the non-linear feasibility constraints on the optimiser, giving priority to feasible solutions. Finally, the optimised buckling loads are shown in Table 3 normalised by the analytical quasi-isotropic (QI) solution. Both the classical and mapped optimisation results are shown to significantly improve the plate resistance to buckling with respect to the QI and the standard  $\pm 45^\circ$  laminate solutions.

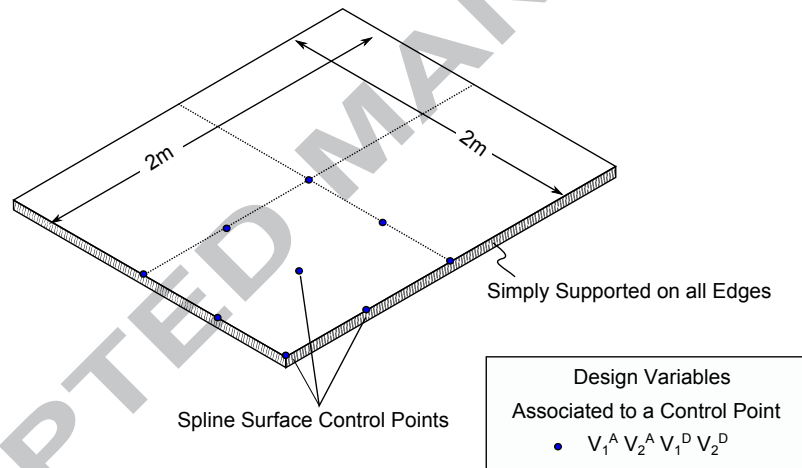


Fig. 16 Structural Optimisation Example

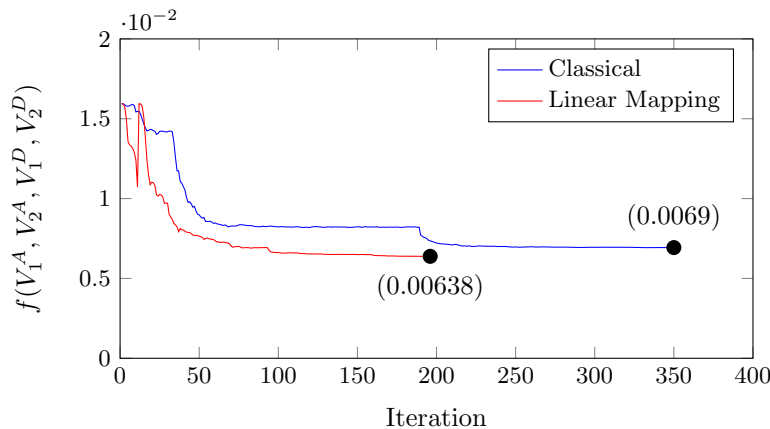
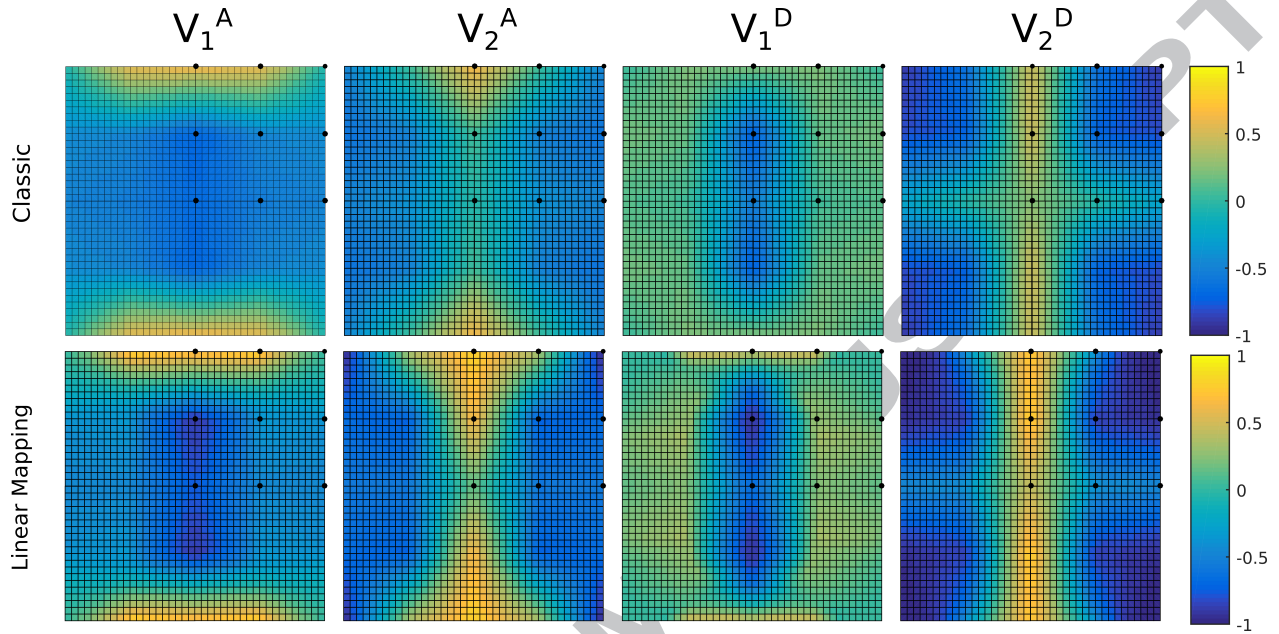


Fig. 17 Structural results comparing the classic and linear mapping optimisation

**Table 3** Structural Optimisation Results

	Analytical $QI$	$QI$	$\pm 45^\circ$	Classical	Linear Map
Normalised Buckling Load	1	1.0089	1.2712	2.3200	2.5195

**Fig. 18** Classical and linear mapping optimisation results

## 5. Concluding Remarks

This work successfully demonstrates the application of feasibility maps to the lamination parameter space. We have shown that maps can ensure lamination parameter feasibility at each optimisation step without the need for computationally expensive feasibility constraints. However, creating suitable maps for the optimisation of lamination parameters is found to be somewhat challenging and the application presented in this paper were limited to four dimensions. Although the effects of these feasibility maps on large structural optimisation problems remain to be investigated, results presented herein suggest that the removal of feasibility constraints leads to faster optimisations.

In this study a generic B-spline mapping procedure that is independent of the number of lamination parameter constraints is proposed. While, in theory, the B-spline map could be used in the 12-dimensional lamination parameter space, the computational cost required in order to compute a sufficiently accurate high dimensional mesh and mapping has proven to be problematic. On the other hand, the linear map is computationally cheap and effective but requires careful manipulation of the lamination parameter feasibility constraints, a task that may also prove difficult in higher dimensions. Future work will include the development of higher dimensional maps able to capture coupling between 8 and 12 lamination parameters. Furthermore, an open-source code for the generation of these mappings will be provided.



## Acknowledgements

The authors would like to acknowledge the support of the EPSRC under its SUPERGEN Wind Challenge 2015 Grant, EP/N006127/1.

## References

- [1] Hossein Ghiasi, Kazem Fayazbakhsh, Damiano Pasini, and Larry Lessard. Optimum stacking sequence design of composite materials part ii: Variable stiffness design. *Composite Structures*, 93(1):1–13, 2010.
- [2] Daniel MJ Peeters, François-Xavier Irisarri, and Mostafa Abdalla. Optimizing the ply dropping order in variable stiffness, variable thickness laminates using stacking sequence tables. In *ECCM17*, 2016.
- [3] Raphael T Haftka and Ramana V Grandhi. Structural shape optimization - a survey. *Computer methods in applied mechanics and engineering*, 57(1):91–106, 1986.
- [4] Yi M Xie and Grant P Steven. A simple evolutionary procedure for structural optimization. *Computers & structures*, 49(5):885–896, 1993.
- [5] F-X Irisarri, Alexis Lasseigne, F-H Leroy, and Rodolphe Le Riche. Optimal design of laminated composite structures with ply drops using stacking sequence tables. *Composite Structures*, 107:559–569, 2014.
- [6] Marco Montemurro. The polar analysis of the third-order shear deformation theory of laminates. *Composite Structures*, 131:775–789, 2015.
- [7] Zhangming Wu, Gangadharan Raju, and Paul M Weaver. Framework for the buckling optimization of variable-angle tow composite plates. *AIAA Journal*, 53(12):3788–3804, 2015.
- [8] Terence Macquart, Noud Werter, and Roeland De Breuker. Aeroelastic tailoring of blended composite structures using lamination parameters. In *57th AIAA/ASCE/AHS/ASC Structures, Structural Dynamics, and Materials Conference*, page 1966, 2016.
- [9] Olivia Stodieck, Jonathan E Cooper, PM Weaver, and Paul Kealy. Optimization of tow-steered composite wing laminates for aeroelastic tailoring. *AIAA Journal*, 53(8):2203–2215, 2015.
- [10] Marco Tito Bordogna, Terence Macquart, Dimitri Bettebghor, and Roeland De Breuker. Aeroelastic optimization of variable stiffness composite wing with blending constraints. In *17th AIAA/ISSMO Multidisciplinary Analysis and Optimization Conference*, page 4122, 2016.
- [11] Terence Macquart, Marco T Bordogna, Paul Lancelot, and Roeland De Breuker. Derivation and application of blending constraints in lamination parameter space for composite optimisation. *Composite Structures*, 2015.
- [12] JL Grenestedt and P Gudmundson. Layup optimization of composite material structures. *Optimal design with advanced materials*, pages 311–336, 1993.
- [13] MW Bloomfield, CG Diaconu, and PM Weaver. On feasible regions of lamination parameters for lay-up optimization of laminated composites. In *Proceedings of the Royal Society of London A: Mathematical, Physical and Engineering Sciences*, pages rspa–2008. The Royal Society, 2008.
- [14] Stephen W Tsai and Nicholas J Pagano. Invariant properties of composite materials. Technical report, DTIC Document, 1968.
- [15] Hong T Hahn and Stephen W Tsai. *Introduction to composite materials*. CRC Press, 1980.
- [16] Zafer Gürdal, Raphael T Haftka, and Prabhat Hajela. *Design and optimization of laminated composite materials*. John Wiley & Sons, 1999.

- [17] Mitsunori Miki and Yoshihiko Sugiyamat. Optimum design of laminated composite plates using lamination parameters. *AIAA journal*, 31(5):921–922, 1993.
- [18] Terence Macquart. Optibless an open-source toolbox for the optimisation of blended stacking sequences. In *17th European Conference on Composite Materials (ECCM17)*, 2016.

ACCEPTED MANUSCRIPT